The Planetary Science Journal, 1:79 (15pp), 2020 December https://doi.org/10.3847/PSJ/abc476

Recovery and Validation of Venus Neutral Atmospheric Profiles from Pioneer Venus Orbiter Radio Occultation Observations

Paul Withers[1,2], Kerry Hensley[1], Marissa F. Vogt[2], and Jacob Hermann[3]
[1] Astronomy Department, Boston University, 725 Commonwealth Avenue, Boston, MA 02215, USA
[2] Center for Space Physics, Boston University, 725 Commonwealth Avenue, Boston, MA 02215, USA
[3] University of Colorado, Boulder, CO 80309, USA
Received 2020 July 9; revised 2020 September 12; accepted 2020 October 21; published 2020 December 17

Abstract

The Pioneer Venus Orbiter radio occultation experiment acquired vertical profiles of neutral atmospheric temperature in the ionosphere of Venus. These profiles were not readily accessible to researchers. Here we report the recovery and validation of a set of neutral atmospheric temperature profiles from Pioneer Venus Orbiter. More than 40 profiles spanning many latitudes and local solar times were deemed acceptable for scientific analysis. These temperature profiles are consistent with temperature profiles measured by the four Pioneer Venus entry probes. The profiles are publicly available and ready for use in scientific investigations of the neutral atmosphere of Venus and related topics.

Unified Astronomy Thesaurus concepts: Venus (1763)

1. Introduction

Pioneer Venus was one of NASA's most successful planetary science missions (Colin 1977; Mutch 1980; Hunten et al. 1983; Bougher et al. 1997). Its orbiter and atmospheric entry probes conducted the first comprehensive study of the atmosphere of another planet. Pioneer Venus Orbiter (PVO), which operated at Venus from 1978 to 1992, determined the composition, structure, and energetics of the neutral upper atmosphere and ionosphere of Venus. It also determined how the plasma environment around Venus is produced by the interaction of the solar wind with Venus.

PVO carried a radio occultation investigation (ORO, led by the late Arv Kliore of JPL) that produced two main data products: vertical profiles of the ionospheric electron density and vertical profiles of the neutral atmospheric temperature and pressure (Kliore et al. 1979a, 1979b, 1991; Berman & Ramos 1980; Kliore & Patel 1980, 1982; Cravens et al. 1981; Woo et al. 1982, 1989; Newman et al. 1984; Kliore 1985, 1992; Kliore & Mullen 1989, 1990; Kliore & Luhmann 1991; Woo & Kliore 1991; Zhang et al. 1990; Brace & Kliore 1991).

Raw radio occultation data from PVO are archived at https://pds-ppi.igpp.ucla.edu/archive1/PV04_0001/ to PV04_0066/. Unfortunately, the high-level data products of the PVO radio occultation investigation, the ionospheric and neutral atmospheric profiles, are not archived at the NASA Planetary Data System (PDS). These ionospheric and neutral atmospheric profiles are not currently available to the scientific community in a digital format. As part of a wide-ranging program to acquire and archive profiles from radio occultation experiments (Withers et al. 2015, 2020; Dalba & Withers 2019), we conducted a search for the PVO radio occultation neutral atmospheric temperature and pressure profiles. The aim of this article is to report the successful recovery and validation of many of these profiles. The recovered profiles and comprehensive documentation are available at https://hdl.handle.net/2144/41269. In 2020 August, this material was delivered to the PDS for review and archiving.

The structure of this article is as follows. Section 2 outlines the scientific value of radio occultation profiles at Venus. Section 3 assesses the availability of neutral atmospheric profiles at Venus from other experiments. Section 4 describes the availability of data from PVO radio occultations. Section 5 validates the neutral atmospheric profiles by comparing National Space Science Data Center (NSSDC) and graphical neutral atmospheric profiles for the same occultation. Section 6 reports an overview of the neutral atmospheric profiles. Section 7 presents the conclusions of this project.

2. The Scientific Value of Radio Occultation Profiles at Venus

Venus and Earth began as twins, possessing near-identical sizes and densities, yet a less Earth-like environment than present-day Venus is hard to imagine. Venus is hellishly hot, devoid of oceans, apparently lacking plate tectonics, and immersed in a thick, reactive atmosphere. How, why, and when did the evolutionary paths of Earth and Venus diverge?

Such questions prompted a sustained program of Soviet exploration and the NASA Pioneer Venus and Magellan missions. More recently, ESA's Venus Express orbiter operated successfully at Venus from 2006 to 2014 and Japan's Akatsuki/Planet-C Venus Climate Orbiter mission entered orbit in 2015. Although NASA has not launched a mission to Venus for 30 yr, the US planetary science community maintains a strong interest in continued exploration of Venus, as demonstrated by the activities of VEXAG, the NASA-chartered Venus Exploration Analysis Group, and the regular submission of strongly rated Venus mission proposals to the NASA Discovery program. For example, two Venus mission concepts (VERITAS and DAVINCI) were selected for Phase A studies in the NASA Discovery program in 2015 and 2020.

Radio occultation data at Venus are relevant to several of the 10 Priority Questions identified by the 2011 Planetary Science Decadal Survey:

3. What governed...the evolution of [inner planet] atmospheres? (E.g., what is the current state of the Venus atmosphere?)

9. Can understanding the roles of physics, chemistry, geology, and dynamics in driving planetary atmospheres lead to a better understanding of climate change on Earth? (E.g., what can be learnt about the greenhouse effect from the atmosphere of Venus?)

Examples of focused science questions that can be answered using the PVO radio occultation data and that are aligned with the strategic goals of NASA's Planetary Science Division include the following:

1. Has the climate of Venus changed between the PVO era and the present day?
2. How consistent are measurements of thermal structure from entry probes (Seiff et al. 1980) and radio occultation experiments?

3. Availability of Neutral Atmospheric Profiles at Venus from Other Experiments

Atmospheric profiles from the four Pioneer Venus entry probes are tabulated in Seiff et al. (1980). Temperature–pressure data from the PVO infrared radiometer (OIR) have never been archived (Taylor et al. 1983). The best OIR data set held by the NSSDC contains temperatures at 70, 80, and 90 km (http://nssdc.gsfc.nasa.gov/nmc/datasetDisplay.do?id=PSPA-00075), which provides notably worse range and resolution than the radio occultation profiles. Six neutral atmospheric profiles from the Magellan radio occultation experiment have been archived (https://pds-atmospheres.nmsu.edu/PDS/data/mg_2401/). In the modern era, access to several hundred neutral atmospheric profiles from the Venus Express radio occultation experiment can be requested from the experimenters (http://www.radio-science.eu/?page_id=746&lang=en), but these profiles have not yet been formally archived (Häusler & Pätzold et al. 2006; Pätzold et al. 2007). Neutral atmospheric profiles from the Venus Express UV spectrometer have not been archived (Piccialli et al. 2015). Sixty-eight neutral atmospheric profiles from the Akatsuki radio occultation experiment have been archived (https://atmos.nmsu.edu/PDS/data/vcors_2001/; Ando et al. 2017, 2018, 2020; Imamura et al. 2017).

The recovery of neutral atmospheric profiles from the PVO radio occultation investigation would significantly increase the number of such profiles available for scientific analysis. This would also enable studies of temporal variations in the neutral atmosphere (e.g., climatological timescales). Moreover, it would improve spatial coverage in terms of latitude and time of day.

4. Availability of Data from PVO Radio Occultations

Many observations were acquired by PVO ORO. Kliore (1985) described 123 neutral atmospheric profiles. PVO's valuable radio occultation neutral atmospheric profiles were never archived at the PDS nor disseminated outside the team. The last publications to use these data appeared over 30 yr ago (Kliore 1985). These data have never been available for comparison to Venus Express or Akatsuki observations.

As part of a wide-ranging program to acquire and archive profiles from radio occultation experiments, we conducted a search for PVO's radio occultation neutral atmospheric profiles. The PDS does hold the raw data (Original Data Records, ODRs) from PVO's radio occultations (https://pds-ppi.igpp.ucla.edu/archive1/PV04_0001/ to PV04_0066/). However, these raw data are very raw, processing them would require a great deal of ancillary information that may not exist, and any effort to process them would be long, hard, and uncertain of success.

The NSSDC provided us with a copy of data set PSPA-00345 (http://nssdc.gsfc.nasa.gov/nmc/datasetDisplay.do?id=PSPA-00345). This data set, which was previously identified as 78-051A-20A, included a set of UNIVAC binary files and one PDF document (hereafter PSPA-00345.pdf). As described more fully in Appendix A, 22 representations of neutral atmospheric profiles were recovered from this data set. Furthermore, figures in Kliore & Patel (1980) contain 10 representations of profiles, and figures in Kliore & Patel (1982) contain 24 representations of profiles. We label profiles recovered from the NSSDC data set as "NSSDC" profiles and profiles recovered from published figures as "graphical" profiles. For some occultations, only a single representation was found. For other occultations, multiple representations were found. This is described more fully in Appendix A. There are 56 representations of neutral atmospheric profiles from 42 occultations (Table 1).

Here we summarize the data recovery process. More comprehensive descriptions are available in Appendix A and in the documentation available with the data products at https://hdl.handle.net/2144/41269.

First, we discuss the data recovery process for the NSSDC profiles. The UNIVAC binary files that were provided by the NSSDC were converted to ASCII files by the Boston University Research Computing Support Center. Three types of data products were recovered: time series of frequency, vertical profiles of ionospheric electron density, and vertical profiles of neutral atmospheric temperature. This article discusses the neutral atmospheric profiles. With the exception of two temperature values discussed in Section 5 that exceed thousands of Kelvin, the temperature profiles are plausible and deemed accurate. Point-to-point fluctuations of tens of Kelvin are common at high altitudes. These fluctuations are likely the expected consequence of the experimenters applying the equation of hydrostatic equilibrium to derive pressure values from a vertical profile of noisy neutral density values. The pressure profiles are also plausible and deemed accurate.

Uncertainties in the temperature and pressure values reported for a given neutral atmospheric profile vary with altitude. Uncertainties decrease as radial distance decreases. Kliore & Patel (1982) estimated the temperature uncertainty to be 1.5 K at the 1 bar pressure level. Data users are referred to the original publications for further discussion of uncertainties in the neutral atmospheric profiles.

Second, we discuss the data recovery process for the graphical profiles. PDF copies of Kliore & Patel (1980, 1982) were obtained. Digital files of selected figures were extracted from these articles. For each profile in each of the selected figures, a set of numerical values of temperature and altitude/pressure was recovered using the "DataThief" tool (https://datathief.org). Altitude in the figures of Kliore & Patel (1982) is referenced to a radial distance of 6052 km (Kliore & Patel 1982). We added 0.2 km to all values of altitude to adjust to a reference radius of 6051.8 km (Archinal et al. 2011).

Table 1
Available Representations of Observations

Observation	Representations
6X	NQ, K80
9N	NQ, K80
18N	NS, NX, K80
18X	NQ
19N	NS, NX
19X	NS, NX
20X	K82
21N	NQ
21X	NQ
22N	NQ
26X	K82
27X	K82
29N	NQ, K80
30X	NQ, K80
32N	K82*
40X	K82
45X	NQ, K80
47X	K82
48N	K82*
48X	K82
51X	K80
56N	NQ, K80
57N	K82
58X	K82
59N	NQ
60N	NQ
61N	NQ
62N	K82
63N	NQ
66X	K82
67N	NQ, K80
69X	NQ, K80
338N	K82
340N	K82
350X	K82
354N	K82
679N	K82
679X	K82
1013X	K82
1027N	K82
1041X	K82
1055N	K82

Note. Observations are identified by the orbit number followed by either "N" (ingress occultation) or "X" (egress occultation). For example, 6X identifies the egress occultation on orbit 6 and 1055N identifies the ingress occultation on orbit 1055. Representations are identified by a series of characters. "NQ" identifies a profile from the NSSDC that is probably *S* band, "NS" identifies an *S*-band NSSDC profile, "NX" identifies an *X*-band NSSDC profile, "K80" identifies a profile present once in Kliore & Patel (1980), "K82" identifies a profile present once in Kliore & Patel (1982), and "K82*" identifies a profile present twice in Kliore & Patel (1982). The only observations present twice in Kliore & Patel (1982) are the ingress occultation on orbit 32, which is shown in their Figures 2 and 10, and the ingress occultation on orbit 48, which is shown in their Figures 2 and 11.

Each profile is labeled by orbit number and whether the observation corresponds to an ingress or egress occultation. It is necessary to generate additional ancillary information to support the analysis and interpretation of these neutral atmospheric observations, including the time of the observation, Venuscentric latitude, Venuscentric east longitude, local solar time, and solar zenith angle. We generated this information using SPICE.

All profiles contain a set of temperature values. Some profiles contain sets of pressure and altitude values, some profiles contain a set of pressure values, but no altitude values, and some profiles contain a set of altitude values, but no pressure values. As the dependence of pressure on altitude in the Venus atmosphere varies across the planet (e.g., Seiff et al. 1980), it is not possible to unambiguously recreate missing pressure values or missing altitude values. Consequently, figures in this article that show vertical temperature profiles use either pressure or altitude for the vertical coordinate, but do not show both quantities.

5. Comparison of NSSDC and Graphical Neutral Atmospheric Profiles for the Same Occultation

Comparison of NSSDC and graphical profiles for the same occultation provides insight into errors that may have been introduced in the graphical recovery process. However, we caution that the PVO experimenters may have used different versions of a profile for NSSDC delivery and for publication in articles. For example, the data-processing pipeline may have evolved between the generation of one version and the generation of the other version. Despite this caveat, comparison of duplicate profiles remains useful.

Nine of the 10 profiles published in Kliore & Patel (1980) are also contained in the NSSDC data set. The exception is the egress occultation on orbit 51. Table 2 lists these profiles, the rms difference in temperature values, and latitude from SPICE.

Figure 1 shows profiles for the egress occultation on orbit 69. The basic shapes of the two representations are similar, although slight offsets are apparent. The rms difference in temperature is 5 K.

Figure 2 shows profiles for the egress occultation on orbit 45. The basic shapes of the two representations are similar, although slight offsets are apparent at low pressure. The rms difference in temperature is 4 K. Yet it is clear from inspection of Figure 2 of Kliore & Patel (1980) that the graphical and NSSDC representations of this profile are inherently different. In the NSSDC representation of this profile, the temperature gradient $dT/d\ln p$ is uniform between pressures of 1 and 100 mbar. This is not the case for the representation shown in Figure 2 of Kliore & Patel (1980), where the temperature gradient changes noticeably around 3 mbar.

Figure 3 shows profiles for the egress occultation on orbit 30. The basic shapes of the two representations are very similar. The rms difference in temperature is 2 K.

Figure 4 shows profiles for the ingress occultation on orbit 67. The basic shapes of the two representations are very similar. The rms difference in temperature is 2 K. Two temperature values of several thousand Kelvin occur near the top of the NSSDC representation of this profile. These are unphysical and should be set aside by data users. They are a consequence of the uncertain upper boundary conditions adopted by the experimenters when generating pressure and temperature profiles from the associated density profile (e.g., Withers et al. 2014). This is an extreme example; more modest scatter visible at the highest altitudes in other NSSDC profiles is caused by the same effect. The graphical profiles do not extend to such high altitudes and consequently do not show this sensitivity to boundary conditions.

Table 2
Neutral Atmospheric Profiles for which Both NSSDC and Graphical Representations Exist

Graphical	NSSDC	rms Difference (K)	Latitude (°N)
k80_02_01	pvoro_nssdc_temp_0069_x_ol_q_v01_r00.tab	5	−4.18
k80_02_03	pvoro_nssdc_temp_0045_x_ol_q_v01_r00.tab	4	−31.00
k80_02_04	pvoro_nssdc_temp_0030_x_ol_q_v01_r00.tab	2	−45.33
k80_02_05	pvoro_nssdc_temp_0067_n_ol_q_v01_r00.tab	2	58.96
k80_02_06	pvoro_nssdc_temp_0006_x_ol_q_v01_r00.tab	4	−60.07
k80_02_07	pvoro_nssdc_temp_0056_n_ol_q_v01_r00.tab	2	70.48
k80_02_08	pvoro_nssdc_temp_0009_n_ol_q_v01_r00.tab	16	83.88
k80_02_09	pvoro_nssdc_temp_0018_n_ol_s_v01_r00.tab	5	86.12
k80_02_10	pvoro_nssdc_temp_0029_n_ol_q_v01_r00.tab	4	86.95

Note. All graphical representations are from Figure 2 of Kliore & Patel (1980).

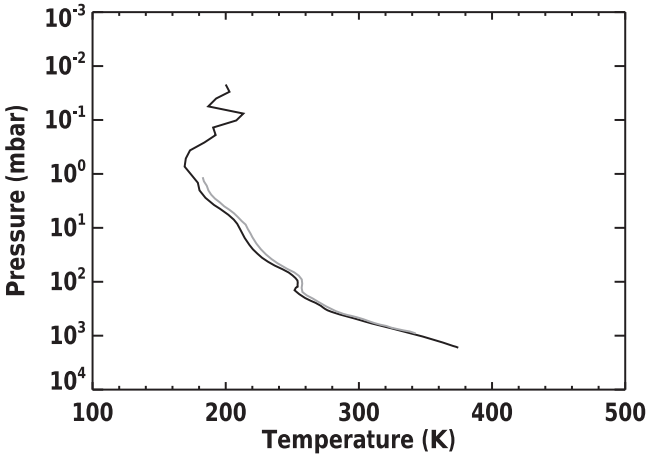

Figure 1. Two representations of the neutral atmospheric profile from the egress occultation on orbit 69. The black line shows the NSSDC representation, and the gray line shows the graphical representation.

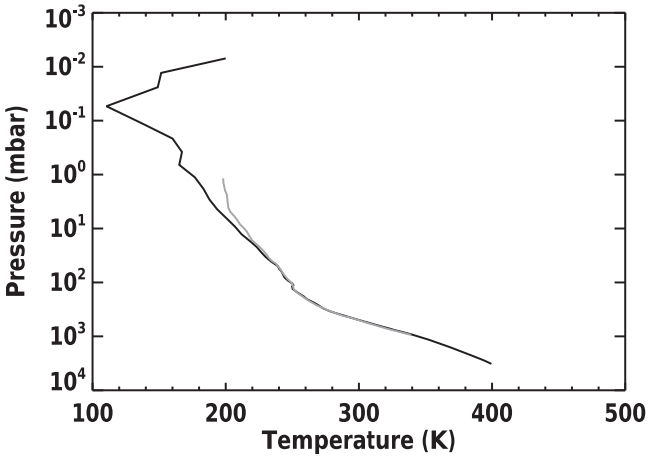

Figure 2. Two representations of the neutral atmospheric profile from the egress occultation on orbit 45. The black line shows the NSSDC representation, and the gray line shows the graphical representation.

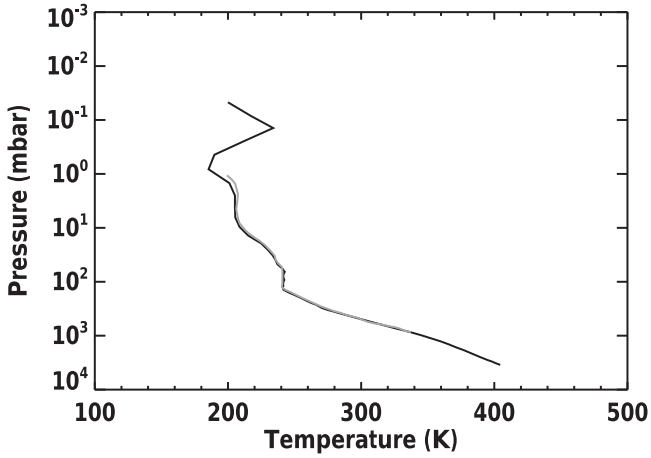

Figure 3. Two representations of the neutral atmospheric profile from the egress occultation on orbit 30. The black line shows the NSSDC representation, and the gray line shows the graphical representation.

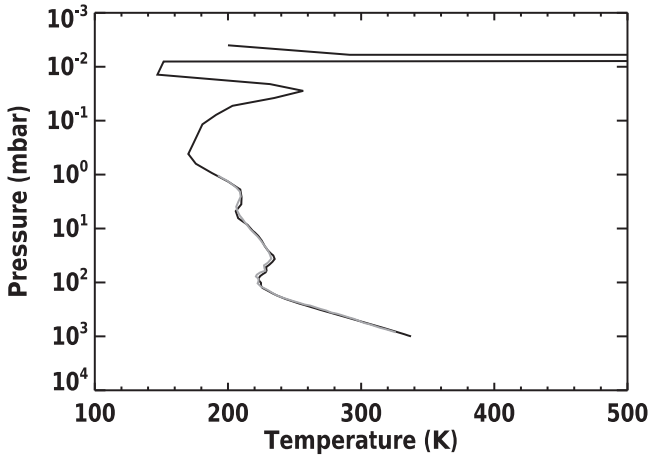

Figure 4. Two representations of the neutral atmospheric profile from the ingress occultation on orbit 67. The black line shows the NSSDC representation, and the gray line shows the graphical representation.

Figure 5 shows profiles for the egress occultation on orbit 6. The basic shapes of the two representations are similar, although slight offsets are apparent. The rms difference in temperature is 4 K.

Figure 6 shows profiles for the ingress occultation on orbit 56. The basic shapes of the two representations are very similar. The rms difference in temperature is 2 K.

Figure 7 shows profiles for the ingress occultation on orbit 9. The basic shapes of the two representations are similar, although large offsets are apparent at low pressures. The rms difference in temperature is 16 K. Yet it is clear from inspection of Figure 2 of Kliore & Patel (1980) that the graphical and NSSDC representations of this profile are inherently different. In the NSSDC representation of this profile, the temperature

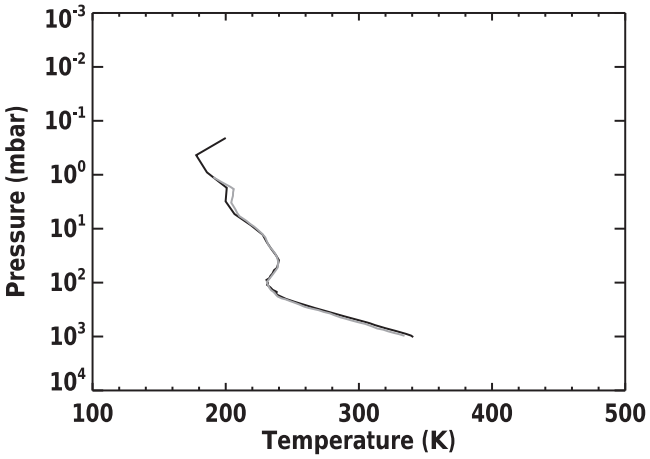

Figure 5. Two representations of the neutral atmospheric profile from the egress occultation on orbit 6. The black line shows the NSSDC representation, and the gray line shows the graphical representation.

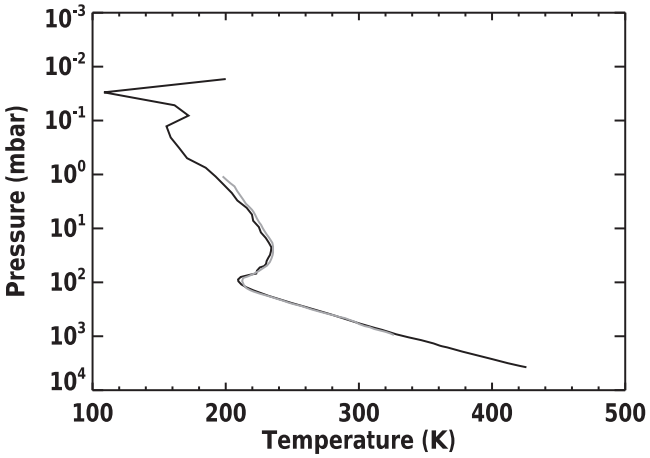

Figure 6. Two representations of the neutral atmospheric profile from the ingress occultation on orbit 56. The black line shows the NSSDC representation, and the gray line shows the graphical representation.

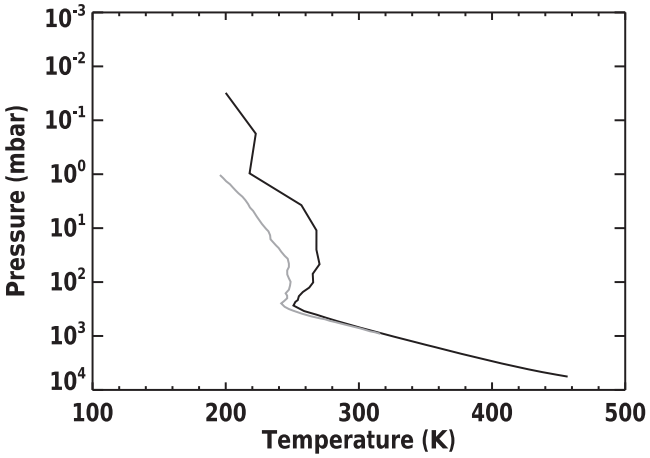

Figure 7. Two representations of the neutral atmospheric profile from the ingress occultation on orbit 9. The black line shows the NSSDC representation, and the gray line shows the graphical representation.

exceeds 265 K between pressures of 10 and 100 mbar. This is not the case for the representation shown in Figure 2 of Kliore & Patel (1980), where the temperature at these pressures is slightly less than 250 K.

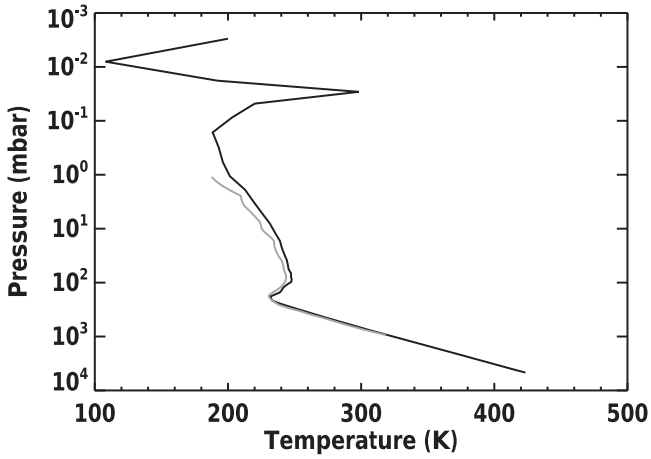

Figure 8. Two representations of the neutral atmospheric profile from the ingress occultation on orbit 18. The black line shows the NSSDC representation, and the gray line shows the graphical representation.

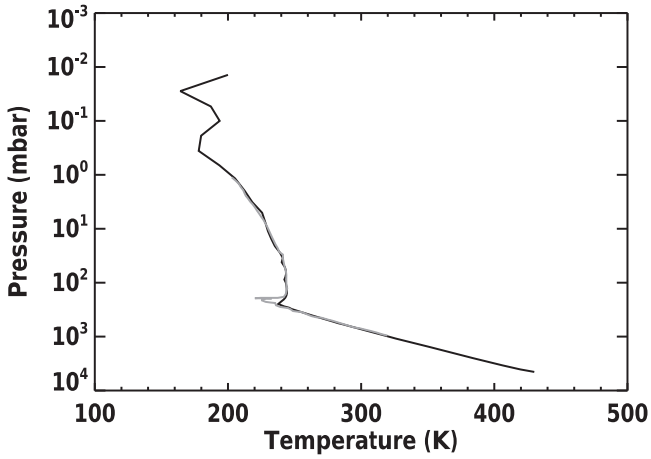

Figure 9. Two representations of the neutral atmospheric profile from the ingress occultation on orbit 29. The black line shows the NSSDC representation, and the gray line shows the graphical representation.

Figure 8 shows profiles for the ingress occultation on orbit 18. The basic shapes of the two representations are similar, although slight offsets are apparent. The rms difference in temperature is 5 K.

Figure 9 shows profiles for the ingress occultation on orbit 29. The basic shapes of the two representations are very similar, except for the region around 200 mbar. Here the temperature in the graphical profile changes abruptly by 20 K. Yet it is clear from inspection of Figure 2 of Kliore & Patel (1980) that the graphical and NSSDC representations of this profile are inherently different. The abrupt change in temperature is noticeable in the representation shown in Figure 2 of Kliore & Patel (1980), but no comparable abrupt change in temperature is present in the NSSDC representation of this profile. The rms difference in temperature is 4 K. If the region around 200 mbar is excluded from this calculation, then the rms difference in temperature decreases to 2 K.

In some instances, it is very clear that the PVO experimenters used different versions of a profile for NSSDC delivery and for publication in Kliore & Patel (1980). Even where differences are not obvious, it is possible that different versions were used. Thus, all of the temperature differences listed above

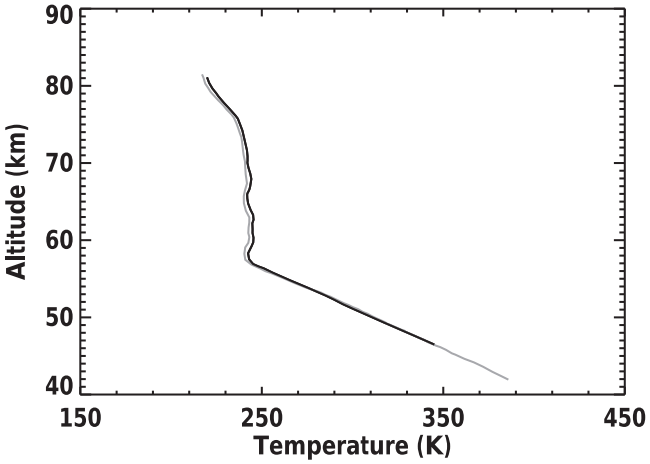

Figure 10. Two representations of the neutral atmospheric profile from the ingress occultation on orbit 32. The black line was recovered from Figure 2 of Kliore & Patel (1982). The gray line was recovered from Figure 10 of Kliore & Patel (1982).

may include contributions from inherent differences as well as from errors in the graphical recovery process.

Further insight into the accuracy of the recovered neutral atmospheric profiles can be obtained by examination of the two representations of the ingress occultation on orbit 32, which was shown in both Figures 2 and 10 of Kliore & Patel (1982). The two recovered representations of this temperature profile are shown in Figure 10. The rms difference in temperature is less than 2 K, comparable to the 1.5 K uncertainty noted by Kliore & Patel (1982) for temperatures at the 1 bar pressure level. The representation recovered from Figure 10 of Kliore & Patel (1982) extends to appreciably lower altitudes than the representation recovered from Figure 2 of Kliore & Patel (1982). This difference in vertical extent can be verified by inspection of these figures in Kliore & Patel (1982)

Based on these considerations, we conclude that the graphical recovery process may have introduced errors of 3 K into the recovered dayside temperature profiles.

6. Overview of Neutral Atmospheric Profiles

Figure 11 shows the latitude and local solar time coverage of the neutral atmospheric profiles. Coverage is dense poleward of 60°N at local solar times between 15 and 24 hr and between the equator and 60°S at local solar times within a few hours of midnight, but is sparse elsewhere. These neutral atmospheric profiles can be compared against the vertical profiles of temperature, pressure, and altitude measured in situ by the four Pioneer Venus probes (Seiff et al. 1980).

Figures 12 and 13 show entry profiles from the night (28.°7S) and day (31.°2S) probes. The profile of the night probe does not sample high altitudes (low pressure) due to unreliable accelerometer data (Seiff et al. 1980). These figures also show all NSSDC and graphical profiles between 20°S and 40°S. There is one NSSDC profile—the egress occultation on orbit 45. There are two graphical profiles from Kliore & Patel (1980; temperature–pressure, egress occultations on orbits 45 and 51) and five graphical profiles from Kliore & Patel (1982; temperature–altitude, egress occultations on orbits 40, 47, 48, 350, and 1041). Figure 12 shows that temperature–pressure profiles from the night probe, day probe, the one relevant NSSDC observation, and the two relevant graphical observations are consistent. Figure 13

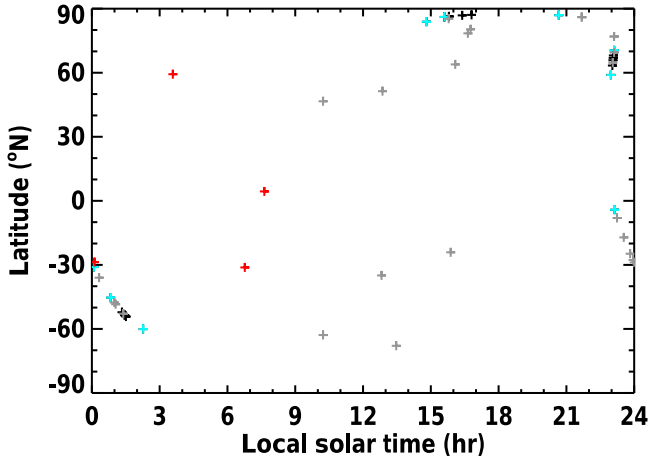

Figure 11. Latitude and local solar time coverage of neutral atmospheric observations. Black symbols show NSSDC observations. Gray symbols show graphical observations. Cyan symbols show observations with both NSSDC and graphical representations. Red symbols show the four Pioneer Venus entry probes.

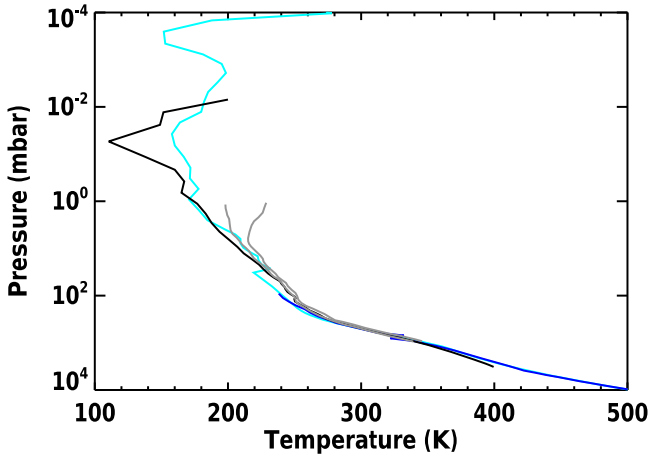

Figure 12. Selected temperature–pressure profiles. The blue and cyan lines show the Pioneer Venus night and day probes, respectively. The black line shows the NSSDC profile from the egress occultation on orbit 45. The gray lines show the graphical profiles from the egress occultations on orbits 45 and 51.

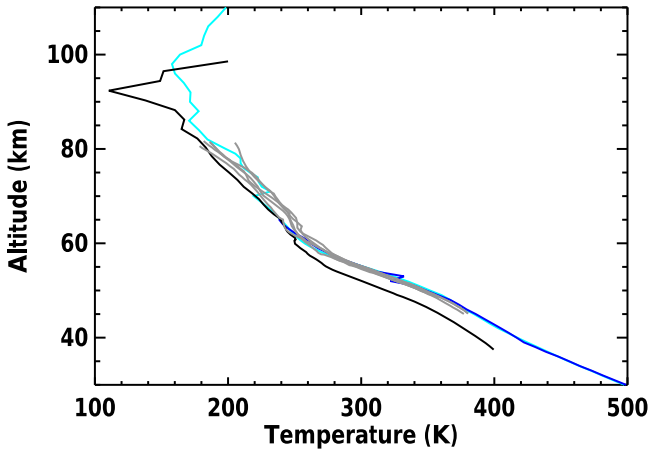

Figure 13. Selected temperature–altitude profiles. The blue and cyan lines show the Pioneer Venus night and day probes, respectively. The black line shows the NSSDC profile from the egress occultation on orbit 45. The gray lines show the graphical profiles from the egress occultations on orbits 40, 47, 48, 350, and 1041.

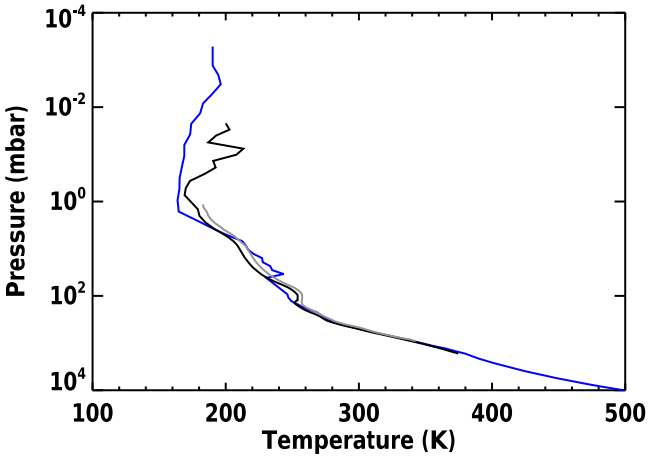

Figure 14. Selected temperature–pressure profiles. The blue line shows the Pioneer Venus sounder probe. The black line shows the NSSDC profile from the egress occultation on orbit 69. The gray line shows the graphical profile from the egress occultation on orbit 69.

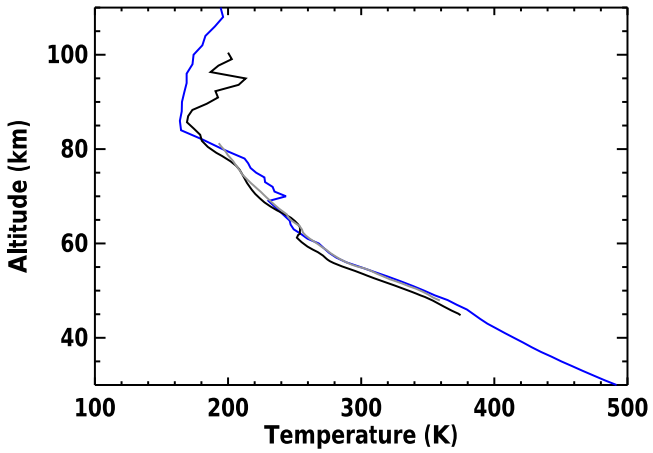

Figure 15. Selected temperature–altitude profiles. The blue line shows the Pioneer Venus sounder probe. The black line shows the NSSDC profile from the egress occultation on orbit 69. The gray line shows the graphical profile from the egress occultation on orbit 66.

shows that temperature–altitude profiles from the night probe, day probe, and the two relevant graphical observations are consistent at tropospheric altitudes, yet the relevant NSSDC observation is not. If altitude values in the relevant NSSDC observation were increased by 3 km, then this temperature–altitude profile would be consistent with the others at tropospheric altitudes.

Figures 14 and 15 show the entry profile from the sounder (4°.4N) probe. These figures also show all NSSDC and graphical profiles between 10°S and 10°N. There is one NSSDC profile—the egress occultation on orbit 69. There is one graphical profile from Kliore & Patel (1980; temperature–pressure, egress occultation on orbit 69) and one graphical profile from Kliore & Patel (1982; temperature–altitude, egress occultation on orbit 66). Figure 14 shows that temperature–pressure profiles from the sounder probe, the one relevant NSSDC observation, and the one relevant graphical observation are consistent. Figure 15 shows that temperature–altitude profiles from the sounder probe and the one relevant graphical observation are consistent at tropospheric altitudes, yet the relevant NSSDC observation is not. If altitude values in the relevant NSSDC observation were increased by 1–2 km, then this temperature–altitude profile would be consistent with the others at tropospheric altitudes.

Figures 16 and 17 show the entry profile from the north (59°.3N) probe. These figures also show all NSSDC and graphical profiles between 55°N and 65°N. There are two NSSDC profiles—the ingress occultations on orbits 63 and 67. There is one graphical profile from Kliore & Patel (1980; temperature–pressure, ingress occultation on orbit 67) and two graphical profiles from Kliore & Patel (1982; temperature–altitude, ingress occultations on orbits 62 and 354). Figure 16 shows that temperature–pressure profiles from the north probe, the two relevant NSSDC observations, and the one relevant graphical observation are consistent. Figure 17 shows that temperature–altitude profiles from the north probe and the two relevant graphical observations are consistent at tropospheric altitudes, yet the relevant NSSDC observations are not. If altitude values in the relevant NSSDC observations were decreased by 1–2 km, then these temperature–altitude profiles would be consistent with the others at tropospheric altitudes.

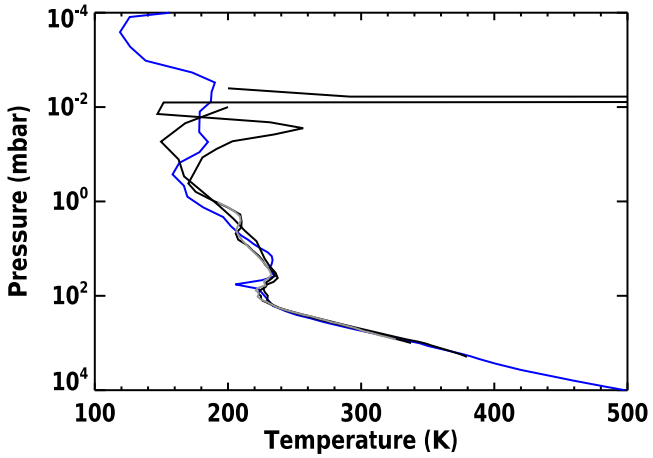

Figure 16. Selected temperature–pressure profiles. The blue line shows the Pioneer Venus north probe. The black lines show the NSSDC profile from the ingress occultations on orbits 63 and 67. The gray line shows the graphical profile from the ingress occultation on orbit 67.

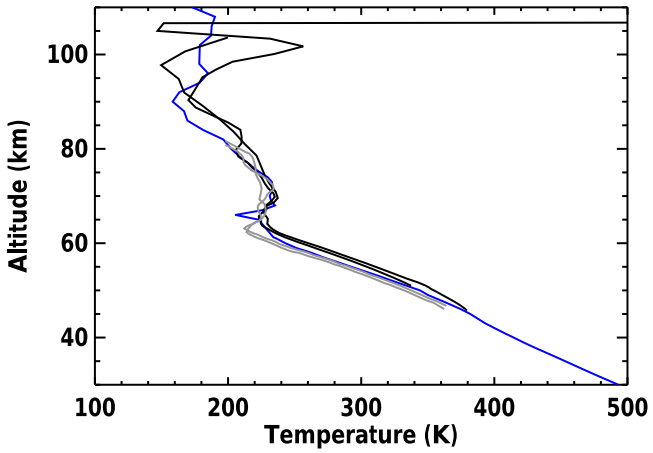

Figure 17. Selected temperature–altitude profiles. The blue line shows the Pioneer Venus north probe. The black lines show the NSSDC profiles from the ingress occultations on orbits 63 and 67. The gray lines show the graphical profiles from the ingress occultation on orbits 62 and 354.

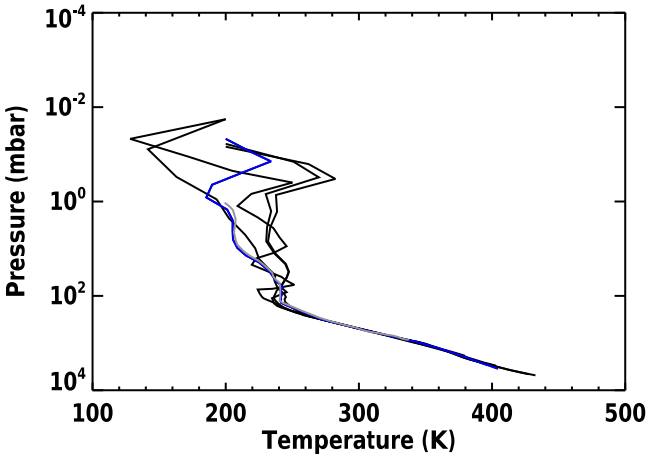

Figure 18. Selected temperature–pressure profiles. The black lines show the NSSDC profiles from the egress occultations on orbits 18, 19 (separate representations for the *S* band and the *X* band), and 21. The blue line shows the NSSDC profile from the egress occultation on orbit 30. The gray line shows the graphical profile from the egress occultation on orbit 30.

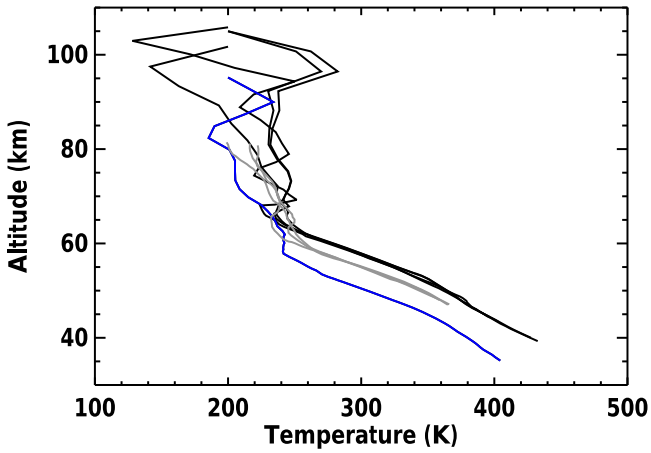

Figure 19. Selected temperature–altitude profiles. The black lines show the NSSDC profiles from the egress occultations on orbits 18, 19 (separate representations for the *S* band and the *X* band), and 21. The blue line shows the NSSDC profile from the egress occultation on orbit 30. The gray lines show the graphical profiles from the egress occultations on orbits 20, 26, and 27.

Figure 11 shows that there are several clusters of NSSDC and graphical profiles at similar latitudes and local solar times. These clusters also provide insight into the reliability of the neutral atmospheric profiles.

Figures 18 and 19 show profiles with latitudes between 55°S and 45°S and local solar times between 0 and 2 hr. There are five NSSDC profiles—the egress occultations on orbits 18, 19 (separate representations for the *S* band and *X* band), 21, and 30. There is one graphical profile from Kliore & Patel (1980; temperature–pressure, egress occultation on orbit 30) and three graphical profiles from Kliore & Patel (1982; temperature–altitude, egress occultations on orbits 20, 26, and 27). Figure 18 shows that temperature–pressure profiles from the five relevant NSSDC observations and the one relevant graphical observation are consistent at tropospheric altitudes. Figure 19 shows that temperature–altitude profiles from the three relevant graphical observations are self-consistent at tropospheric altitudes. Yet temperature–altitude profiles from the the five relevant NSSDC observations are not self-consistent at tropospheric altitudes. If altitude values in the NSSDC egress occultation on orbit 30 were increased by 7 km, then the NSSDC observations would be self-consistent at tropospheric altitudes. However, they would still not be consistent with the graphical observations at tropospheric altitudes. If altitude values in the NSSDC egress occultation on orbit 30 were increased by 4 km and altitude values in the other four NSSDC observations were decreased by 3 km, then NSSDC and graphical temperature–altitude profiles would be consistent at tropospheric altitudes.

Figures 20 and 21 show profiles with latitudes between 60°N and 75°N and local solar times between 22 and 24 hr. There are five NSSDC profiles—the ingress occultations on orbits 56, 59, 60, 61, and 63. There is one graphical profile from Kliore & Patel (1980; temperature–pressure, ingress occultation on orbit 56) and two graphical profiles from Kliore & Patel (1982; temperature–altitude, ingress occultations on orbits 57 and 62). Figure 20 shows that temperature–pressure profiles from the five relevant NSSDC observations and the one relevant graphical observation are consistent. Figure 21 shows that temperature–altitude profiles from the two relevant graphical

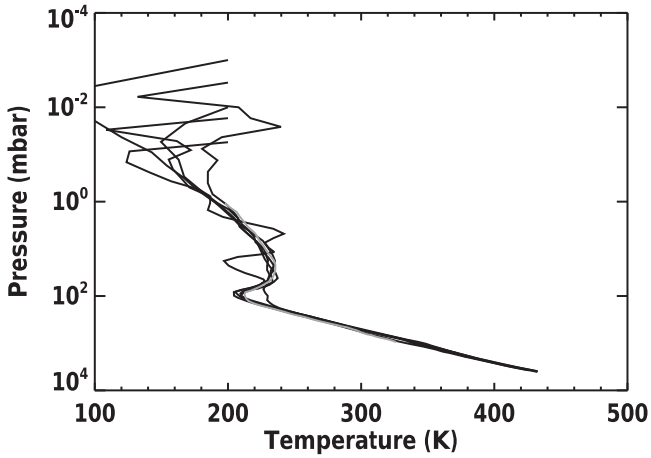

Figure 20. Selected temperature–pressure profiles. The black lines show the NSSDC profiles from the ingress occultations on orbits 56, 59, 60, 61, and 63. The gray line shows the graphical profile from the ingress occultation on orbit 56.

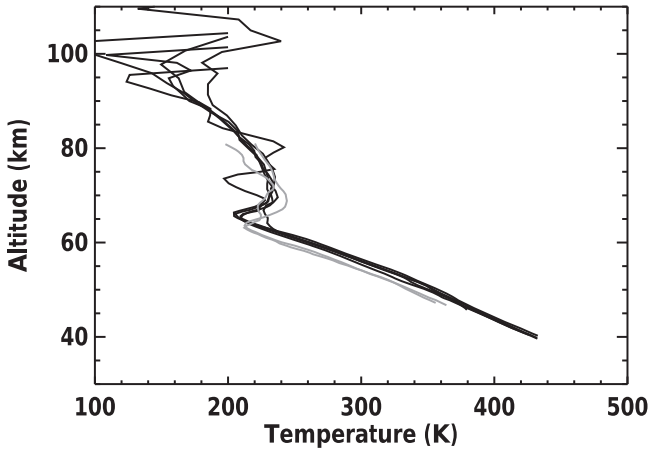

Figure 21. Selected temperature–altitude profiles. The black lines show the NSSDC profiles from the ingress occultations on orbits 56, 59, 60, 61, and 63. The gray lines show the graphical profiles from the ingress occultations on orbits 57 and 62.

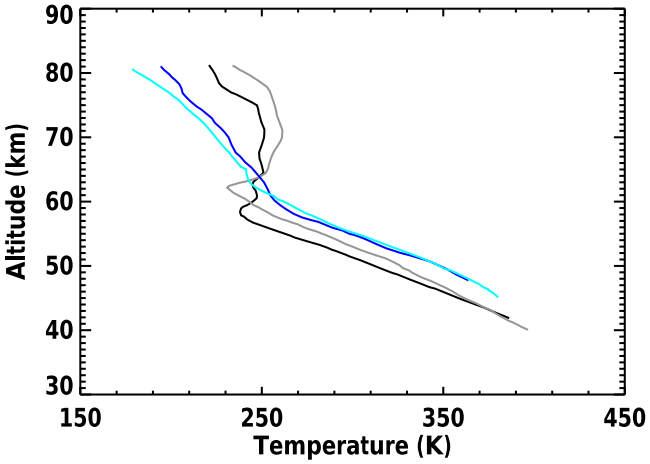

Figure 22. Four selected graphical neutral atmospheric profiles with local solar times between 12 and 16 hr. The black profile shows the ingress occultation on orbit 1027 (85.°28N). The gray profile shows the egress occultation on orbit 1013 (67.°91S). The blue profile shows the ingress occultation on orbit 1055 (51.°37N). The cyan profile shows the egress occultation on orbit 350 (24.°12S).

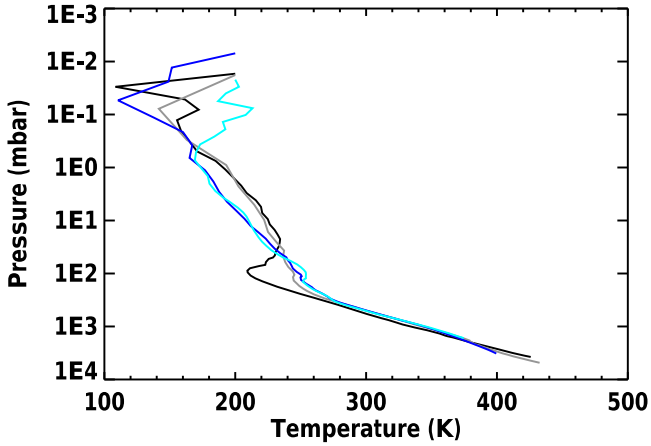

Figure 23. Four selected NSSDC temperature–pressure profiles with local solar times within two hours of midnight. The black profile shows the ingress occultation on orbit 56 (70.°48N). The gray profile shows the egress occultation on orbit 21 (52.°17S). The blue profile shows the egress occultation on orbit 45 (31.°00S). The cyan profile shows the egress occultation on orbit 69 (4.°18S).

observations are self-consistent at tropospheric altitudes, the five relevant NSSDC observations are self-consistent at tropospheric altitudes, but the NSSDC and graphical observations are not consistent at tropospheric altitudes. If altitude values in the relevant NSSDC observations were decreased by 2 km, then the NSSDC and graphical observations would be consistent at tropospheric altitudes.

Temperature–pressure profiles from NSSDC and graphical sources appear to be reliable. Temperature–altitude profiles from graphical sources also appear to be reliable. Yet NSSDC temperature–altitude profiles do not appear to be as reliable. The stated altitude values appear to contain errors of several kilometers. We advise that values of altitude in NSSDC profiles be treated with caution by data users.

As discussed in Section 5, some, perhaps all, neutral atmospheric profiles were reprocessed between the delivery of profiles to the NSSDC and the publication of Kliore & Patel (1982). The NSSDC documentation is dated 1981 January 20 and Kliore & Patel (1982) has a manuscript revision date of 1982 August 30, an ample 19 month interval for reprocessing. The requirements imposed on data collection and processing capabilities by PVO radio occultations were significantly more stringent than those of earlier missions (Berman & Ramos 1980; Kliore & Patel 1980). Therefore, it is plausible that the initial implementation of these capabilities was assessed and modified after delivery of profiles to the NSSDC, leading to improvements in the profiles generated at later dates.

Figures 12–17 also show that variations in atmospheric thermal structure with local solar time are small at the pressures and altitudes sampled by radio occultations (Taylor et al. 1983). Figures 12 and 13 illustrate this with data from two entry probes, one NSSDC profile, and seven graphical profiles (20°S to 40°S). These data sample local solar times around 0, 7, 13, and 16 hr. Figures 14 and 15 illustrate this with data from one entry probe, one NSSDC profile, and two graphical profiles (10°S to 10°N). These data sample local solar times around 8 and 23 hr. Figures 16 and 17 illustrate this with data from one entry probe, two NSSDC profiles, and three graphical profiles (55°N to 65°N). These data sample local solar times around 4, 16, and 23 hr.

Conversely, variations in atmospheric thermal structure with latitude are substantial (e.g., Kliore & Patel 1982; Limaye et al. 2018). Figure 22 shows four graphical profiles from local solar times between 12 and 16 hr. The midlatitude profiles at 24.°12S and 51.°37N are similar. Here, temperature decreases monotonically with increasing altitude, and no distinct tropopause temperature minimum is visible. In the convective lower atmosphere, the midlatitude profiles are warmer than the near-polar profiles at 67.°91S and 85.°28N. Conversely, in the radiative middle atmosphere, the midlatitude profiles are cooler than the near-polar profiles. The near-polar profiles do contain distinct tropopause temperature minima.

Figure 23 shows four NSSDC profiles from local solar times within two hours of midnight. The near-equatorial profiles at 31.°00S and 4.°18S are similar. The midlatitude profile at 52.°17S is similar to these two profiles at high pressures, but is warmer at pressures less than 30 mbar. In these three profiles, temperature decreases monotonically with decreasing pressure and no distinct tropopause temperature minimum is visible. The near-polar profile at 70.°48N is similar to the other three in the deep atmosphere but contains a deep tropopause temperature minimum around 100 mbar where it is appreciably cooler than the other three profiles. Yet it is similar to the midlatitude profile at pressures less than 30 mbar.

Figure 24 illustrates the dependence of temperature in the graphical profiles on altitude and latitude. We do not include the NSSDC temperature–altitude profiles due to the unreliability of their altitude values, which was addressed earlier in this section. The use of the absolute value of latitude here, which assumes hemispheric symmetry, is justified shortly. Each pixel indicates the average value of temperature within a region of 5° extent in solar zenith angle and 2 km extent in altitude. To construct this figure, each temperature profile was interpolated onto a common altitude grid. The value shown in a pixel of the figure is the average of all interpolated temperature measurements at that altitude which have solar zenith angles within the appropriate range. Two gaps in the coverage of the graphical profiles are filled using data from the Pioneer Venus sounder (4.°4N) and north (59.°3N) probes. These two entry probe profiles have much greater vertical extent than the graphical profiles used in the majority of this figure. Figure 24 is accompanied by Figure 25, which illustrates how temperature depends on latitude at several fixed altitudes.

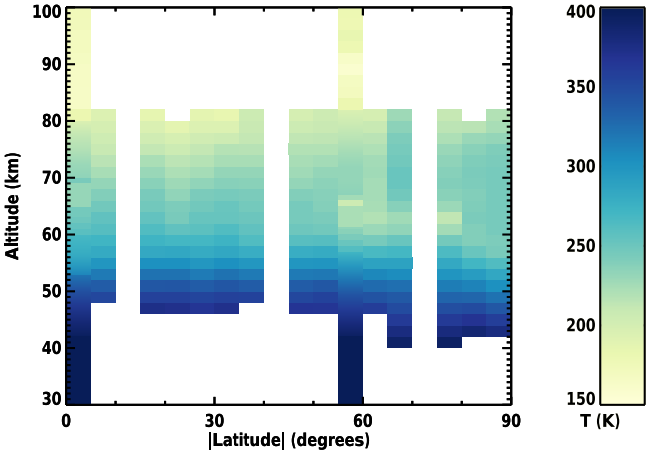

Figure 24. Dependence of temperature in the graphical profiles on altitude and latitude. Two gaps in the coverage of the graphical profiles are filled using data from the Pioneer Venus sounder (4.°4N) and north (59.°3N) probes. Regions without data are shown in white.

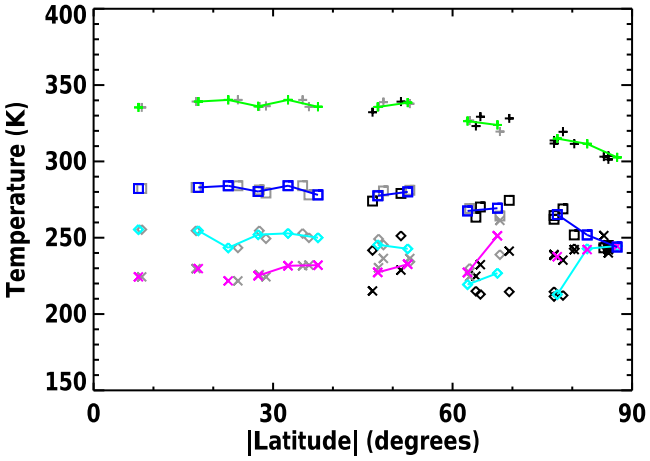

Figure 25. Dependence of temperature in the graphical profiles on latitude at selected altitudes. Symbols indicate altitude. Plus signs indicate 50 km altitude. Squares indicate 56 km altitude. Diamonds indicate 62 km altitude. Multiplication signs indicate 70 km altitude. Observations from the Northern Hhemisphere are shown by black symbols. Observations from the Southern Hemisphere are shown by gray symbols. Averaged temperatures from Figure 24 are shown by colored symbols. Green indicates 50 km altitude. Blue indicates 56 km altitude. Cyan indicates 62 km altitude. Magenta indicates 70 km altitude. No data from Pioneer Venus entry probes are shown in this figure.

Overall, temperature variations with altitude are more significant than those with latitude. At low altitudes, temperature tends to decrease from equator to pole. At high altitudes, the opposite occurs and temperature tends to decrease from equator to pole. The transition occurs around 63 km altitude, where temperature is relatively constant with altitude—except for a region of appreciably cooler temperatures around 60°N–80°N. This is known as the "cold collar" region (e.g., Taylor et al. 1983; Crisp & Titov 1997; Sánchez-Lavega et al. 2017; Limaye et al. 2018).

Similarly, Figures 26 and 27 illustrate the dependence of temperature in the NSSDC profiles on pressure and latitude. The vertical extent of each pixel in Figure 26 is $d \log_{10} p = 0.1$. One gap in Figure 26 is filled using data from the Pioneer Venus night (28.°7S) probe. This entry probe profile extends to greater pressures than the NSSDC profiles used in the majority of this figure. However, it does not extend to lower pressure due to unreliable accelerometer data (Seiff et al. 1980).

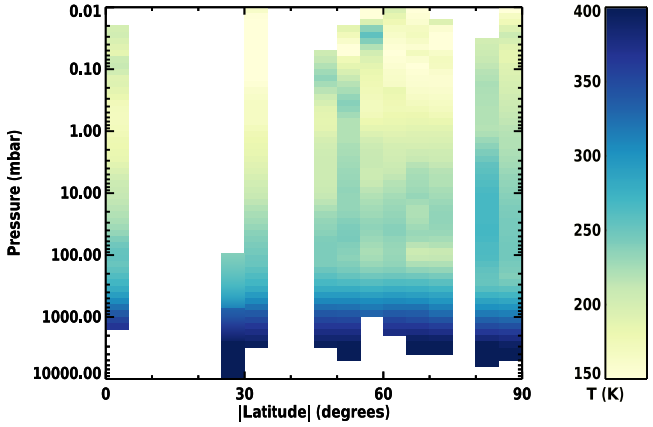

Figure 26. Dependence of temperature in the NSSDC profiles on pressure and latitude. One gap in the coverage of the NSSDC profiles is filled using data from the Pioneer Venus night (28.°7S) probe. Regions without data are shown in white.

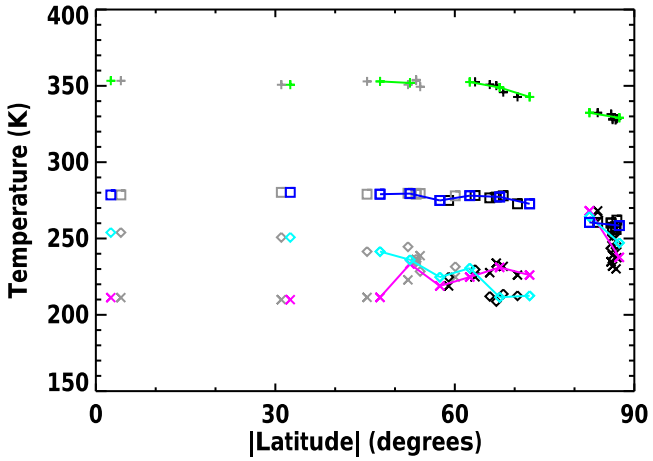

Figure 27. Dependence of temperature in the NSSDC profiles on latitude at selected pressure levels. Symbols indicate pressure level. Plus signs indicate 1000 mbar. Squares indicate 300 mbar. Diamonds indicate 100 mbar. Multiplication signs indicate 10 mbar. Observations from the Northern Hemisphere are shown by black symbols. Observations from the Southern Hemisphere are shown by gray symbols. Averaged temperatures from Figure 26 are shown by colored symbols. Green indicates 1000 mbar. Blue indicates 300 mbar. Cyan indicates 100 mbar. Magenta indicates 10 mbar. No data from Pioneer Venus entry probes are shown in this figure.

Latitudinal coverage is sparser for the NSSDC profiles than for the graphical profiles, but the overall picture is the same. The cold collar region is noticeable at a pressure level of 100 mbar.

Figures 25 and 27 distinguish between the Northern and Southern Hemisphere observations. However, there is no appreciable difference between the temperature measurements in the two hemispheres, which justifies the decision to use the absolute value of latitude in Figures 24–27.

Similar patterns in the thermal structure of the Venus atmosphere have been described in Kliore & Patel (1982), Kliore (1985), Taylor et al. (1983), Crisp & Titov (1997), Sánchez-Lavega et al. (2017), and Limaye et al. (2018).

7. Summary

We have recovered, validated, and archived an extensive set of neutral atmospheric temperature profiles from radio occultations by Pioneer Venus Orbiter. Some neutral atmospheric temperature

profiles were recovered from figures in publications by the PVO experimenters, and some were recovered from files maintained by the NSSDC.

We have recovered 22 representations of NSSDC neutral atmospheric data products, all of which were suitable for archiving. Uncertainties in the temperature and pressure values contained in NSSDC data products decrease as altitude decreases. Kliore & Patel (1982) estimated the temperature uncertainty to be 1.5 K at the 1 bar pressure level. The vertical resolution of the NSSDC neutral atmospheric profiles depends on altitude. It typically decreases from several kilometers at 90 km to 0.5 km at 60 km. Temperature and pressure values in the archived set of NSSDC neutral atmospheric data products are reliable. They are consistent with graphical neutral atmospheric data products and measurements by the Pioneer Venus entry probes. However, altitude values appear to be offset by several kilometers. Data users are advised to be cautious when using values of altitude in NSSDC neutral atmospheric data products.

We have recovered 34 representations of graphical neutral atmospheric data products, all of which were suitable for archiving. No problems were identified in the archived set of graphical neutral atmospheric data products. There are nine neutral atmospheric data products for which both NSSDC and graphical representations exist. Based on comparisons between these pairs of neutral atmospheric data products, we find that the graphical recovery process may have introduced errors of 3 K into the recovered dayside temperature profiles.

In total, 56 representations of neutral atmospheric profiles were recovered from 42 occultations (Table 1). This is comparable to the total number of accessible neutral atmospheric profiles from the Pioneer Venus probes, Magellan, and Akatsuki. It is much smaller than the number of neutral atmospheric profiles acquired by Venus Express, which can be requested from the experimenters.

Overall, the neutral atmospheric data products show the expected trends with altitude, latitude, and local solar time. The recovered profiles and comprehensive documentation are available at https://hdl.handle.net/2144/41269. In 2020 August, this material was delivered to the PDS for review and archiving. These data products are ready for use in scientific investigations of the neutral atmosphere of Venus and related topics. For instance, the neutral atmospheric profiles could be compared with more recent measurements to assess whether the climate of Venus has changed between the PVO era and the present day.

This work was supported, in part, by NASA award NNX17AK95G. We thank Robert Putnam and the Boston University Research Computing Services for extraction of data from the NSSDC package and Casey Flynn for support of the recovery of graphical profiles. We also thank two anonymous reviewers.

Appendix A
Overview

The structure of this appendix is as follows. Appendix B presents the spatial and temporal extent of the PVO radio occultation observations. Appendix C details the neutral atmospheric profiles recovered from files maintained by the NSSDC. It addresses the data recovery process, the content of the neutral atmospheric data files, the preparation and validation of the data, and the assessment of the quality of the data. Appendix D describes the neutral atmospheric profiles recovered from figures in published articles. Appendix E outlines the process by which ancillary information was obtained for these neutral atmospheric profiles.

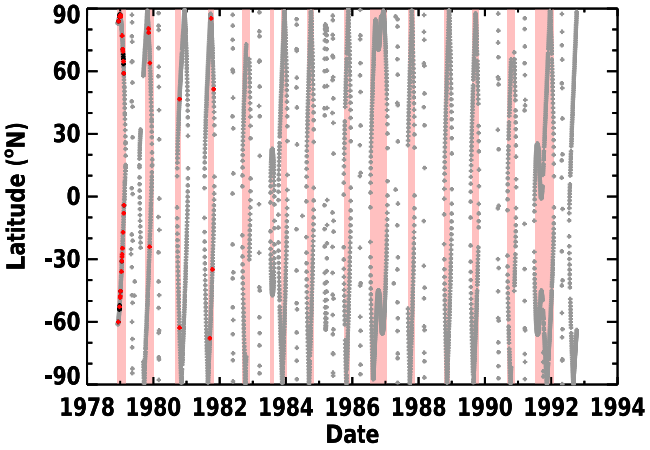

Figure 28. Latitude coverage of PVO occultation opportunities. Gray symbols show all occultation opportunities during the mission. Black symbols show occultations for which NSSDC neutral atmospheric profiles exist. Red symbols show occultations for which graphical neutral atmospheric profiles were recovered. Pink regions show the occultation seasons listed in Table 3.

Appendix B
Spatial and Temporal Extent of PVO Radio Occultation Observations

The SPICE kernels online at http://naif.jpl.nasa.gov/pub/naif/PIONEER12/kernels/spk/ do not cover the full duration of the PVO mission. However, ASCII tables of PVO position in a standard reference frame are available at 12 s resolution from https://pds-ppi.igpp.ucla.edu/data/PVO-V-POS-5–VSOCOORDS-12SEC-V1.0/. Standard SPICE tools were used to generate a low-fidelity trajectory kernel for PVO from these tables. We then used this trajectory kernel to find the times and locations of each occultation point over the complete duration of the PVO mission. The occultation point was defined as the time and location where the ray path of the radio signal transmitted from the spacecraft to Earth has a closest approach distance to Venus equal to the representative ionospheric radial distance of 6200 km. Specifically, we found date and time (OCC_TIME_SPICE), solar zenith angle (SZA_SPICE), areocentric latitude (LAT_SPICE), areocentric east longitude (LON_SPICE), and local solar time (LST_SPICE).

The periods when occultation opportunities occurred are shown in Figure 28. Periods when radio occultation observations were acquired tended to cluster into "occultation seasons." The dates of these occultation seasons can be determined from inspection of the temporal coverage of the raw radio occultation data archived at https://pds-ppi.igpp.ucla.edu/archive1/PV04_0001/ to PV04_0066/. However, this source provides confusing information for occultation seasons 1–4. For these seasons, we adopt the dates stated in Figure 1 of Cravens et al. (1981), supported by Table 1 of Kliore (1985). Note that Table 1 of Kliore (1985) contains a typographical error for season 4 (IV) in which the year is incorrectly specified as 1980. The correct year is 1981. Table 3 provides the dates of the 15 occultation seasons observed by PVO.

Table 3
Occultation Seasons

Season	Start	End
1	December 1978	February 1979
2	October 1979	December 1979
3	September 1980	October 1980
4	September 1981	October 1981
5	10 September 1982	5 December 1982
6	17 July 1983	22 August 1983
7	7 November 1983	11 January 1984
8	18 August 1984	1 November 1984
9	5 October 1985	1 December 1985
10	20 July 1986	18 January 1987
11	10 September 1987	16 November 1987
12	8 October 1988	13 December 1988
13	17 August 1989	26 October 1989
14	7 September 1990	1 December 1990
15	8 July 1991	28 January 1992

Appendix C
NSSDC Neutral Atmospheric Profiles

C.1. Recovery Process

The NSSDC provided us with a copy of data set PSPA-00345 (http://nssdc.gsfc.nasa.gov/nmc/datasetDisplay.do?id=PSPA-00345). This data set, which was previously identified as 78-051A-20A, included a set of UNIVAC binary files and one PDF document (hereafter PSPA-00345.pdf).

The PSPA-00345.pdf document contains two reports written by the PVO ORO team (Kliore and Patel). The first report (3 pages, undated) is titled "Pioneer Venus Orbiter Radio Occultation NSSDC Data Delivery Plan." This describes the initial plan for the content and format of data products. The second report (12 pages, 1981 January 20) is titled "Pioneer Venus Project Radio Science Team Venus Occultation Experiment Reduced Data—Explanatory Document." This states the actual content and format of the delivered data products. The content and format of data products evolved from the initial plan (first report) to actual delivery (second report). As discussed further below, detailed examination of the recovered data products found that some files did not appear to be in their stated format. The document defines three types of data products: type 50, time series of received frequencies, frequency residuals, and power at *S* and *X* bands; type 15, radial profile of ionospheric electron density; and type 16, radial profiles of neutral atmospheric temperature and pressure for upper boundary conditions of 150, 200, and 250 K.

The PSPA-00345.pdf document also lists the delivered data products. The PSPA-00345.pdf document lists 68 groups of files, where each group corresponds to a stated orbit. For each file in a group, the PSPA-00345.pdf document states file type, whether the data are from an ingress or egress occultation, and whether the data were acquired using an open-loop or a closed-loop receiver at the DSN ground station. Although useful, detailed examination of the recovered data products suggested that this list contains some apparent inaccuracies. The first orbit listed is orbit 1 (1978 December 5) and the last orbit listed is orbit 85 (1979 February 27).

The UNIVAC binary files were converted to ASCII files by the Boston University Research Computing Support Center. As expected, 68 groups of files were obtained. Within those groups, there were 225 files. Of these 225 files, there were 109 files identified as type 50, 94 files identified as type 15, and 22 files identified as type 16. Files were assigned local filenames in the format AA-B-CC.txt, where AA identifies the group, B identifies the position of the file within its group, and CC identifies the file type. AA is a two-character number from 01 to 68. The orbit that corresponds to a file can be identified by comparing the group number to the listing of group and orbit numbers in the PSPA-00345.pdf document. This can be done independently of the file's contents. B is a one- or two-character number from 1 to 10. This position usually corresponds to the position of this file in the listing in the PSPA-00345.pdf document. CC is 50, 15, or 60.

As detailed in subsequent sections, errors were identified in the recovered files. The recovery process itself could have introduced some of these errors.

C.2. File Contents, File Headers, and Other Ancillary Information

Type 16 files include a header that states spacecraft identification number (SCID16), orbit number (ORB16), day of year (DOY16), identification number of the DSN antenna that received the downlink signal (DSS16), whether the data products are derived from *S*-band or *X*-band data (BAND16), and whether this was an ingress or an egress observation (MODE16). The body of each type 16 file is divided into three blocks. Data products in the first block were derived using an upper boundary condition of 150 K. Data products in the second block were derived using an upper boundary condition of 200 K. Data products in the third block were derived using an upper boundary condition of 250 K. Each line in a block in the body of a type 16 file states the closest approach distance of this ray path to the center of planet, which is conventionally denoted by the symbol r (RXXX16), refractivity, which is conventionally denoted by the symbol ν (NUXXX16), pressure (PXXX16), temperature (TXXX16), and an index that identifies the data point. Here, "XXX" is "150," "200," or "250" corresponding to the appropriate upper boundary condition. Throughout this report, we use data products with the 200 K boundary conditions unless otherwise stated. There were typically on the order of 70 lines of data in each block of a type 16 file.

For each recovered file, we identified the file type, orbit number, ingress/egress, whether its data were derived from closed-loop or open-loop data, and whether its data were derived from *S*-band data, *X*-band data, or both. File type was identified by comparison of the actual file format to the templates defined for the three file types in PSPA-00345.pdf document. Orbit number, ingress or egress, and frequency band (s) were identified using the file header and verified using any available supporting information. Whether a file's data were derived from closed-loop or open-loop data was not explicitly stated in any of the three file types. All type 16 files are derived from open-loop data, which was determined by inspection of the listing in the PSPA-00345.pdf document and confirmed in Kliore & Patel (1980, 1982). The resultant assignments are listed in Table 4.

Each file was matched to its corresponding occultation time and location as predicted by SPICE using the date and orbit number information contained within the file. These were verified by comparison to Table 1 of Cravens et al. (1981), which lists orbit number, date, latitude, solar zenith angle, and whether the occultation was ingress or egress. As the PVO

Table 4
Type 16 Files

Orbit Number	Mode	Loop	Band	Local Filename
06	X	OL	*Q*	05-3-16.txt
09	N	OL	*Q*	07-2-16.txt
18	N	OL	*S*	12-4-16.txt
18	N	OL	*X*	12-5-16.txt
18	X	OL	*Q*	12-8-16.txt
19	X	OL	*X*	13-10-16.txt
19	N	OL	*S*	13-6-16.txt
19	N	OL	*X*	13-7-16.txt
19	X	OL	*S*	13-9-16.txt
21	N	OL	*Q*	15-3-16.txt
21	X	OL	*Q*	15-6-16.txt
22	N	OL	*Q*	16-6-16.txt
29	N	OL	*Q*	21-4-16.txt
30	X	OL	*Q*	22-1-16.txt
45	X	OL	*Q*	35-5-16.txt
56	N	OL	*Q*	46-2-16.txt
59	N	OL	*Q*	49-5-16.txt
60	N	OL	*Q*	50-5-16.txt
61	N	OL	*Q*	51-3-16.txt
63	N	OL	*Q*	53-5-16.txt
67	N	OL	*Q*	56-4-16.txt
69	X	OL	*Q*	58-4-16.txt

Note. Mode is N for ingress or X for egress. Loop is CL for closed-loop and OL for open-loop. Band is *S* for *S* band, X for *X* band, Q for "probably *S* band," and D for both *S* and *X* bands.

orbital period was almost 24 hr during this epoch, no ambiguities arose in this process.

C.3. Preparation and Verification of Type 16 Files

We retained all 22 type 16 files.

First, we consider the headers of these files (SCID16, ORB16, DOY16, DSS16, BAND16, MODE16).

All values of SCID16 were 12.

In files 07-2-16.txt (pvoro_nssdc_temp_0009_n_ol_q_v01_r00.tab) and 56-4-16.txt (pvoro_nssdc_temp_0067_n_ol_q_v01_r00.tab), ORB16 is erroneously given as 0, a null value. We replaced these with the correct values of 9 and 67, respectively, which were determined using the group number/orbit number listing in the PSPA-00345.pdf document. For 56-4-16.txt (pvoro_nssdc_temp_0067_n_ol_q_v01_r00.tab), this value could be confirmed against orbit numbers in other files in its group. Corrected values for ORB16 were between 6 and 69.

The most common value of DSS16 is 14. A value of 43 is also present for five of the later occultations.

All values of BAND16 are 3. The meaning of this value of BAND16 is not defined in the PSPA-00345.pdf document, but analogy with defined values of BAND50 and BAND15 suggests that it means that data in a type 16 file is derived from radio signals at both *S*-band and *X*-band frequencies. However, Kliore & Patel (1980) make it clear that the combination of these two bands was used to remove ionospheric effects before a neutral atmospheric profile was determined from measurements at a single frequency. This raises the question of which frequency was used to determine each neutral atmospheric profile. Two type 16 files exist for the ingress occultation on orbit 18, two for the ingress occultation on orbit 19, and two for the egress occultation on orbit 19. For each pair, the listing in the PSPA-00345.pdf document makes it clear that one member of the pair was generated from *S*-band frequency data and the other member was generated from *X*-band frequency data. As Kliore & Patel (1980) note that "*S* band frequency residuals...are generally used to compute the structure of the neutral atmosphere because the *S* band signal is absorbed to a far lesser degree than *X* band in the cloud regions of Venus," we inspected the minimum radial distance reported for each of these six type 16 files. In each pair, the minimum radial distance was 5 km lower in one member than the other member. Therefore, we identified the member with the smallest value of minimum radial distance as the *S*-band profile and the other as the *X*-band profile. The ordering of *S*-band and *X*-band files that resulted from this process matched the ordering stated in the listing in the PSPA-00345.pdf document. Based on the preference of Kliore & Patel (1980) for generating neutral atmospheric profiles using *S*-band frequency data, we identified the 16 other type 16 files as "probably *S* band." This is consistent with the convention stated in the PSPA-00345.pdf document that files derived from *X*-band data are explicitly labeled as such, but files derived from *S*-band data are either explicitly labeled as such or not labeled.

Two-thirds of the MODE16 values are 1 (ingress) and one-third of the MODE16 values are 2 (egress).

Second, we consider the bodies of these files (RXXX16, NUXXX16, TXXX16, PXXX16), where "XXX" is "150," "200," or "250."

Entries in the body of a type 16 file are ordered by radial distance such that values of RXXX16 decrease through the file.

Values of R15016, R20016, and R25016 are identical. Values of RXXX16 are between 6085 km and 6165 km. The typical vertical resolution is 1 km.

Values of NU15016, NU20016, and NU25016 are identical. All values of NUXXX16 are less than 2000. Refractivity is defined as the refractive index minus one. In the type 16 files, the units of NU16 are such that 10^{-6} NU16 equals the refractive index minus one ("N-units"). Neutral refractivity is independent of frequency Withers (2010).

With two exceptions, all values of T20016 are between 50 K and 500 K. The exceptions are in file 56-4-16.txt (pvoro_nssdc_temp_0067_n_ol_q_v01_r00.tab). Two values of several thousand Kelvin occur near the top of this profile. They are a consequence of the experimenters starting the neutral atmospheric profile at a high altitude, where values of neutral density (refractivity) exhibit significant scatter. Pressure and temperature are derived from density using the equation of hydrostatic equilibrium and the ideal gas law. Values of T15016 and T25016 are similar to values of T20016, with differences being consistent with the consequences of adopting different upper boundary conditions. T25016 is greater than T20016, which is greater than T15016. The difference ΔT between T25016 and T20016 can be approximately represented as $\Delta T/K = \text{mbar/P20016}$. Thus, representative differences are 10 K at 10^{-2} mbar and 0.01 K at 10 mbar. Differences between T20016 and T15016 are similar.

All values of P20016 are between 10^{-6} bars and 10 bars. Values of P15016 and P25016 are similar to values of P20016, with differences being less than 0.06 mbar and consistent with the consequences of adopting different upper boundary conditions. P25016 is greater than P20016, which is greater than P15016. The difference Δp between P25016 and P20016 can be approximately represented as $\Delta p/\text{P20016} = 10^{-2}\,\text{mbar/P20016}$. Thus,

representative relative differences are 10^{-6} at 10 bars and 10^{-1} at 0.1 mbar.

Altitude is not included in the type 16 files. We generated an altitude value (ZXXX16) to accompany each value of RXXX16. Altitude was defined as the difference between radial distance and the reference radius of Venus, 6051.8 km (Archinal et al. 2011).

C.4. Quality Assessment of NSSDC Neutral Atmospheric Profiles

With the exception of the couple of temperature values discussed above (Appendix C.3) that exceed thousands of Kelvin, the temperature profiles are plausible and deemed accurate. Point-to-point fluctuations of tens of Kelvin are common at high altitudes. These fluctuations are likely the expected consequence of the experimenters applying the equation of hydrostatic equilibrium to derive pressure values from a vertical profile of noisy neutral density values. The pressure profiles are also plausible and deemed accurate.

Uncertainties in the temperature and pressure values reported for a given neutral atmospheric profile vary with altitude. Uncertainties decrease as radial distance decreases. Kliore & Patel (1982) estimated the temperature uncertainty to be 1.5 K at the 1 bar pressure level. Data users are referred to the original publications for further discussion of uncertainties in the neutral atmospheric profiles.

Appendix D
Graphical Neutral Atmospheric Profiles

Figures in Kliore & Patel (1980) contain 10 neutral atmospheric profiles. These show the dependence of temperature on pressure, but do not show altitude. The pressure range is 1–1000 mbar, and the temperature range is 150–350 K. Figures in Kliore & Patel (1982) contain 24 representations of 23 neutral atmospheric profiles. These show the dependence of temperature on altitude, but do not show pressure. Two observations, the ingress occultations on orbits 32 and 48, are shown twice. The altitude range is 30–90 km, and the temperature range is 150–450 K. There are no profiles that are present in both Kliore & Patel (1980) and Kliore & Patel (1982). PDF copies of Kliore & Patel (1980, 1982) were obtained. Digital files of selected figures were extracted from these articles. For each profile in each of the selected figures, a set of numerical values of temperature and altitude/pressure was recovered using the "DataThief" tool (https://datathief.org).

Altitude in the figures of Kliore & Patel (1982) is referenced to a radial distance of 6052 km (Kliore & Patel 1982). We added 0.2 km to all values of altitude to adjust to a reference radius of 6051.8 km (Archinal et al. 2011). Adjacent profiles often overlapped in the figures of Kliore & Patel (1982), which occasionally made it challenging to assign a data point to a specific profile. However, this was less impactful for the neutral atmospheric profiles than for the ionospheric profiles. Each neutral atmospheric profile in a panel was plotted using a unique style (e.g., solid, dashed, dotted), and the profile shapes were generally smoother for the neutral atmospheric profiles than for ionospheric profiles.

This work was conducted using the generic PDF copies provided at the publisher's website. Toward the end of this project, it was realized that the figures in the library's bound versions of the original journal issues displayed finer details than in these generic PDF copies. Colleagues considering reproducing this work are advised to start from bound versions of the original journal issues themselves, rather than using the generic PDF copies available at the publisher's website.

Appendix E
Ancillary Information for Graphical Neutral Atmospheric Profiles

Each profile is labeled by orbit number and whether the observation corresponds to an ingress or egress occultation. It is necessary to generate additional ancillary information to support the analysis and interpretation of these neutral atmospheric observations, including the time of the observation, Venuscentric latitude, Venuscentric east longitude, local solar time, and solar zenith angle. We generated this information using SPICE.

We matched each recovered profile to an occultation opportunity identified by SPICE as outlined below. All profiles in Kliore & Patel (1980) were acquired in the first PVO occultation season. All profiles in Kliore & Patel (1982) were acquired in the first four PVO occultation seasons. Kliore & Patel (1982) listed the dates and orbit numbers of the beginning and end of each of these seasons. As PVO's orbital period was very close to 24 hr, this information can be used to infer an occultation date from a stated orbit number. This is sufficient to uniquely identify the appropriate opportunity in the list of occultations generated by SPICE. Results were verified using Table 1 of Cravens et al. (1981), which lists orbit number, date, latitude, solar zenith angle, and whether the occultation was ingress or egress for occultations in the first three PVO occultation seasons. Similar tables in Kliore (1985) and Kliore & Mullen (1989) were useful for the fourth PVO occultation season.

There was one exception to this process. The orbit number and ingress/egress information was omitted from one profile in Figure 11 of Kliore & Patel (1982). This profile is identified as being a dayside profile from the fourth PVO occultation season at latitude 67.°6S and solar zenith angle 71.°1. We identified this profile as corresponding to the egress occultation on orbit 1013 because the listing for this occultation in Table 2 of Kliore (1985) has the same values of latitude and solar zenith angle.

All profiles are labeled by latitude, and most profiles are labeled by solar zenith angle. All latitude values listed in figure labels in Kliore & Patel (1980, 1982) are consistent with the corresponding latitude values found by SPICE to within a few degrees. The same is true for most, but not all, of the solar zenith angle values. For the ingress occultation on orbit 1027, Kliore & Patel (1982) stated a solar zenith angle of 118.°1, but SPICE found the solar zenith angle to be 85.°2. Table 1 of Kliore (1985) listed a solar zenith angle of 84.°5 for this observation, which suggests that the value given by Kliore & Patel (1982) is incorrect. For the egress occultation on orbit 1041, Kliore & Patel (1982) stated a solar zenith angle of 98.°8, but SPICE found the solar zenith angle to be 39.°3. Table 1 of Kliore (1985) listed a solar zenith angle of 37.°8 for this observation, which suggests that the value given by Kliore & Patel (1982) is incorrect.

The publications by the PVO ORO experimenters do not precisely define the ray path whose closest approach point was used to provide the published values of latitude and solar zenith angle. Position information in the NSSDC ionospheric data

products (type 15) used the ray path whose radial distance of closest approach was 6200 km, which we adopted in our SPICE calculations of the ionospheric occultations. It is possible that the PVO ORO experimenters used a different ray path to provide position information for the neutral atmospheric profiles. We use the 6200 km reference in our SPICE calculations of the neutral atmospheric occultations. This ensures consistency between ionospheric and neutral atmospheric results.

ORCID iDs

Paul Withers https://orcid.org/0000-0003-3084-4581
Kerry Hensley https://orcid.org/0000-0003-4790-2928
Marissa F. Vogt https://orcid.org/0000-0003-4885-8615

References

Ando, H., Imamura, T., Sugimoto, N., et al. 2017, JGRE, 122, 1687
Ando, H., Imamura, T., Tellmann, S., et al. 2020, NatSR, 10, 3448
Ando, H., Takagi, M., Fukuhara, T., et al. 2018, JGRE, 123, 2270
Archinal, B. A., A'Hearn, M. F., Bowell, E., et al. 2011, CeMDA, 109, 101
Berman, A. L., & Ramos, R. 1980, ITGRS, GE-18, 11
Bougher, S. W., Hunten, D. M., & Phillips, R. J. 1997, Venus II (Tucson, AZ: Univ. Arizona Press)
Brace, L. H., & Kliore, A. J. 1991, SSRv, 55, 81
Colin, L. 1977, SSRv, 20, 249
Cravens, T. E., Kliore, A. J., Kozrya, J. U., & Nagy, A. F. 1981, JGR, 86, 11323
Crisp, D., & Titov, D. 1997, in Venus II : Geology, Geophysics, Atmosphere, and Solar Wind Environment, ed. S. W. Bougher, D. M. Hunten, & R. J. Phillips (Tucson, AZ: Univ. Arizona Press), 353
Dalba, P. A., & Withers, P. 2019, JGRA, 124, 643
Häusler, B., Pätzold, M., Tyler, G. L., et al. 2006, P&SS, 54, 1315
Hunten, D. M., Colin, L., Donahue, T. M., & Moroz, V. I. 1983, Venus (Tucson, AZ: Univ. Arizona Press)
Imamura, T., Ando, H., Tellmann, S., et al. 2017, EP&S, 69, 137
Kliore, A. J. 1985, AdSpR, 5, 41
Kliore, A. J. 1992, in Venus and Mars: Atmospheres, Ionospheres, and Solar Wind Interactions; Proc. of the Chapman Conf., ed. J. G. Luhmann, M. Tatrallyay, & R. O. Pepin (Washington, DC: AGU), 265
Kliore, A. J., & Luhmann, J. G. 1991, JGR, 96, 21281
Kliore, A. J., Luhmann, J. G., & Zhang, M. H. G. 1991, JGR, 96, 11065
Kliore, A. J., & Mullen, L. F. 1989, JGR, 94, 13339
Kliore, A. J., & Mullen, L. F. 1990, AdSpR, 10, 15
Kliore, A. J., & Patel, I. R. 1980, JGR, 85, 7957
Kliore, A. J., & Patel, I. R. 1982, Icar, 52, 320
Kliore, A. J., Patel, I. R., Nagy, A. F., Cravens, T. E., & Gombosi, T. I. 1979a, Sci, 205, 99
Kliore, A. J., Woo, R., Armstrong, J. W., Patel, I. R., & Croft, T. A. 1979b, Sci, 203, 765
Limaye, S. S., Grassi, D., Mahieux, A., et al. 2018, SSRv, 214, 102
Mutch, T. A. 1980, JGR, 85, 7573
Newman, M., Schubert, G., Kliore, A. J., & Patel, I. R. 1984, J. Atmos. Sci., 41, 1901
Pätzold, M., Häusler, B., Bird, M. K., et al. 2007, Natur, 450, 657
Piccialli, A., Montmessin, F., Belyaev, D., et al. 2015, P&SS, 113, 321
Sánchez-Lavega, A., Lebonnois, S., Imamura, T., Read, P., & Luz, D. 2017, SSRv, 212, 1541
Seiff, A., Kirk, D. B., Young, R. E., et al. 1980, JGR, 85, 7903
Taylor, F. W., Hunten, D. M., & Ksanfomality, L. V. 1983, in Venus, ed. D. M. Hunten et al. (Tucson, AZ: Univ. Arizona Press), 650
Withers, P. 2010, AdSpR, 46, 58
Withers, P., Felici, M., Flynn, C., & Vogt, M. F. 2020, PSJ, 1, 14
Withers, P., Moore, L., Cahoy, K., & Beerer, I. 2014, P&SS, 101, 77
Withers, P., Weiner, S., & Ferreri, N. R. 2015, EP&S, 67, 194
Woo, R., Armstrong, J. W., & Kliore, A. J. 1982, Icar, 52, 335
Woo, R., & Kliore, A. J. 1991, JGR, 96, 11073
Woo, R., Sjogren, W. L., Luhmann, J. G., Kliore, A. J., & Brace, L. H. 1989, JGR, 94, 1473
Zhang, M. H. G., Luhmann, J. G., & Kliore, A. J. 1990, JGR, 95, 17095